Intraseasonal variations of the tropical total ozone and their connection to the Madden-Julian Oscillation

B. Tian,[1] Y. L. Yung,[2] D. E. Waliser,[1] T. Tyranowski,[2,3] L. Kuai,[2] E. J. Fetzer,[1] and F. W. Irion[1]

Received 23 January 2007; revised 23 February 2007; accepted 16 March 2007; published 21 April 2007.

[1] We investigate the intraseasonal (30–90 day) variations in satellite-observed tropical total ozone (O_3) and their connection to the Madden-Julian Oscillation (MJO). Tropical total O_3 intraseasonal variations are large (~±10 DU) and comparable to those in annual and interannual time scales. These O_3 anomalies are mainly evident in the subtropics over the Pacific and eastern; hemisphere and propagate slowly eastward (~5 m s^{-1}). The subtropical negative (positive) O_3 anomalies are typically collocated with the subtropical upper troposphere anticyclones (cyclones) generated by equatorial MJO convection and flank or lie to the west of the equatorial enhanced (suppressed) MJO convection. The subtropical O_3 are anti-correlated with geopotential height anomalies near the tropopause and thus mainly associated with the O_3 variability in the stratosphere rather the troposphere. Over the equatorial regions, total O_3 anomalies are small.
Citation: Tian, B., Y. L. Yung, D. E. Waliser, T. Tyranowski, L. Kuai, E. J. Fetzer, and F. W. Irion (2007), Intraseasonal variations of the tropical total ozone and their connection to the Madden-Julian Oscillation, *Geophys. Res. Lett.*, *34*, L08704, doi:10.1029/2007GL029451.

1. Introduction

[2] The Madden-Julian Oscillation (MJO; aka Intraseasonal Oscillation) [*Madden and Julian*, 1972, 1994] is the dominant component of the intraseasonal (30–90 day) variability in the tropical atmosphere. Since its discovery, the MJO has continued to be a topic of significant interest due to its extensive interactions with other components of the climate system and the fact that it represents a connection between the better understood weather and seasonal-to-interannual climate variations. The MJO is characterized by slowly (~5 m s^{-1}) eastward-propagating, large-scale oscillations in the tropical deep convection and baroclinic wind field, especially over the warmest tropical waters in the equatorial Indian and western Pacific Oceans [e.g., *Rui and Wang*, 1990; *Hendon and Salby*, 1994; *Kiladis et al.*, 2001]. Such characteristics tend to be most strongly exhibited during the boreal winter (Nov–Apr) when the Indo-Pacific warm pool is centered near the equator. For more comprehensive reviews of the MJO and related issues, the reader is referred to *Lau and Waliser* [2005]. From the discussion above and cited review materials, it is apparent that the large-scale MJO convection and circulation characteristics have been well documented and in some cases understood. However, the impact of the MJO on intraseasonal variations of atmospheric composition, such as ozone (O_3), has yet to be well documented.

[3] The total column O_3 in the tropical atmosphere depends on both chemical and dynamical processes and has been extensively studied during the last few decades. Previous studies have investigated the tropical total O_3's secular trend [e.g., *Stolarski et al.*, 1992], annual cycle [e.g., *Shiotani*, 1992], and interannual variations associated with the quasi-biennial oscillation (QBO) [e.g., *Bowman*, 1989], El Niño-Southern Oscillation (ENSO) [e.g., *Camp et al.*, 2003], and solar cycle [e.g., *Hood*, 1997]. The tropical total O_3 varies on the order of ±10 Dobson Units (DU) (~3% of the mean) for the annual cycle and ENSO, about ±15 DU (~5% of the mean) for QBO, and about ±5 DU (~2% of the mean) for the solar cycle. However, very few studies have investigated the intraseasonal variations of the tropical total O_3. *Sabutis et al.* [1987] first reported evidence for 30–50 day variability in the Total Ozone Mapping Spectrometer (TOMS) total O_3 over specific locations in the southeast Pacific and southern Indian Oceans. *Gao and Stanford* [1990] found that low-frequency variations with periods of about 1–2 months exist in 8-year TOMS O_3 data. Based on ozonesonde data in Indonesia, *Fujiwara et al.* [1998] suggested that the upper troposphere (UT) O_3 enhancement is tied to the passage of Kelvin waves and the MJO. From estimates of tropospheric O_3 using differential measurements of total O_3 from TOMS and stratospheric O_3 from Microwave Limb Sounder (MLS), *Ziemke and Chandra* [2003] suggested an influence from the MJO on tropospheric O_3. While these studies have investigated the intraseasonal variations of tropical O_3 and suggested tacit connections to the MJO, it is evident that the spatial and temporal patterns of the intraseasonal variations of tropical total O_3 and their connection to the large-scale MJO convection and dynamics have yet to be explained or even comprehensively documented.

[4] This study is to investigate the spatial and temporal patterns of the intraseasonal variations of tropical total O_3 and their connection to the large-scale MJO convection and circulation anomalies. Section 2 introduces the data and methodology and section 3 presents the main results followed by a summary in section 4.

2. Data and Methodology

[5] For this study, we mainly use the daily total O_3 on a 5° × 10° lat-lon grid from a merged ozone data set (MOD)

[1]Jet Propulsion Laboratory, California Institute of Technology, Pasadena, California, USA.
[2]Division of Geological and Planetary Sciences, California Institute of Technology, Pasadena, California, USA.
[3]Institute of Physics, Jagiellonian University, Krakow, Poland.

0094-8276/07/2007GL029451

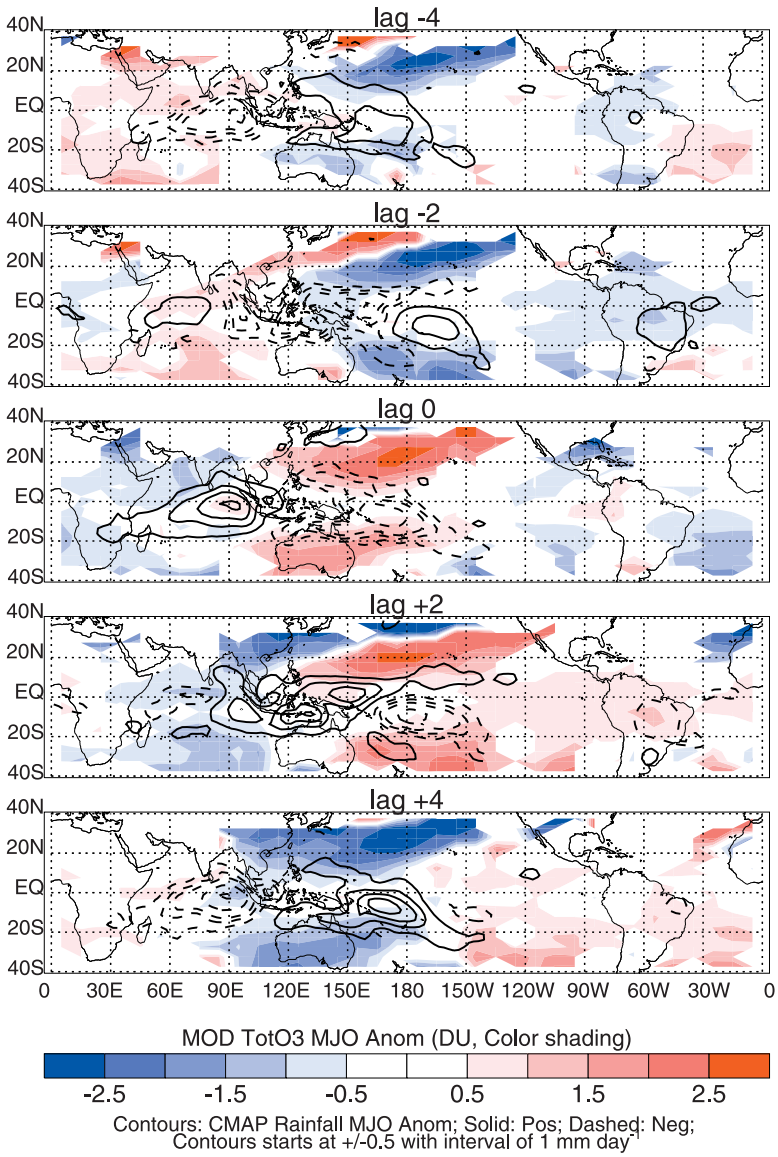

Figure 1. Composite MOD total O_3 (DU, color shading) and CMAP rainfall (mm day^{-1}, black contours) MJO anomalies. For simplicity, only lags ±4, ±2, and 0 pentads of the MJO cycle are shown. Also, only the total O_3 anomalies with above 95% confidence limit are shown.

developed by *Stolarski and Frith* [2006]. The MOD was constructed by combining total O_3 measurements from six satellite instruments: Nimbus-7 TOMS, Nimbus-7 Solar Backscatter Ultraviolet (SBUV), NOAA 9, 11, and 16 SBUV2s, and Earth Probe TOMS. We have used the Version 8 MOD data from Jan 1980 to Jun 2006. The Version 8 TOMS and SBUV has many important improvements from Version 7, such as including aerosol and sea glint corrections, improved retrieval efficiency in the troposphere, and improved a priori O_3 profiles.

[6] The Atmospheric Infrared Sounder (AIRS) [*Chahine et al.*, 2006] O_3 is a research product that is currently undergoing validation. *Gettelman et al.* [2004] compared AIRS O_3 with research aircraft measurements in the UT and suggested AIRS O_3 has a positive bias in the UT. *Randel and Park* [2006] demonstrated that AIRS O_3 can capture the O_3 variability in the UT associated with the Asian summer monsoon anticyclones and deep convection over Southeast Asia. To characterize the ability of AIRS O_3 in capturing the intraseasonal variability, we use AIRS L3-V.4 daily total O_3 product from Sep 2002 to Jul 2006 and on a 5° × 10° lat-lon grid averaged from its original 1° × 1° grid.

[7] To identify MJO events, we use global pentad rainfall data from the NOAA Climate Prediction Center (CPC) Merged Analysis of Precipitation (CMAP) from 1 Jan 1979 to 31 May 2006 on a 2.5° × 2.5° grid. To characterize the large-scale MJO circulation anomalies, daily geopotential height and stream function (calculated from daily horizontal winds) (2.5° × 2.5°, 1979–2006) from the National Centers for Environmental Prediction/National Center for Atmospheric Research reanalysis (NCEP) are used. For the MJO analysis and composite procedure, we use the method of *Tian et al.* [2006]. All data were first binned into 5-day average (i.e. pentad) values. Intraseasonal anomalies were obtained by removing the annual cycle and then band-pass filtering (30–90 day) the data. To isolate the dominant

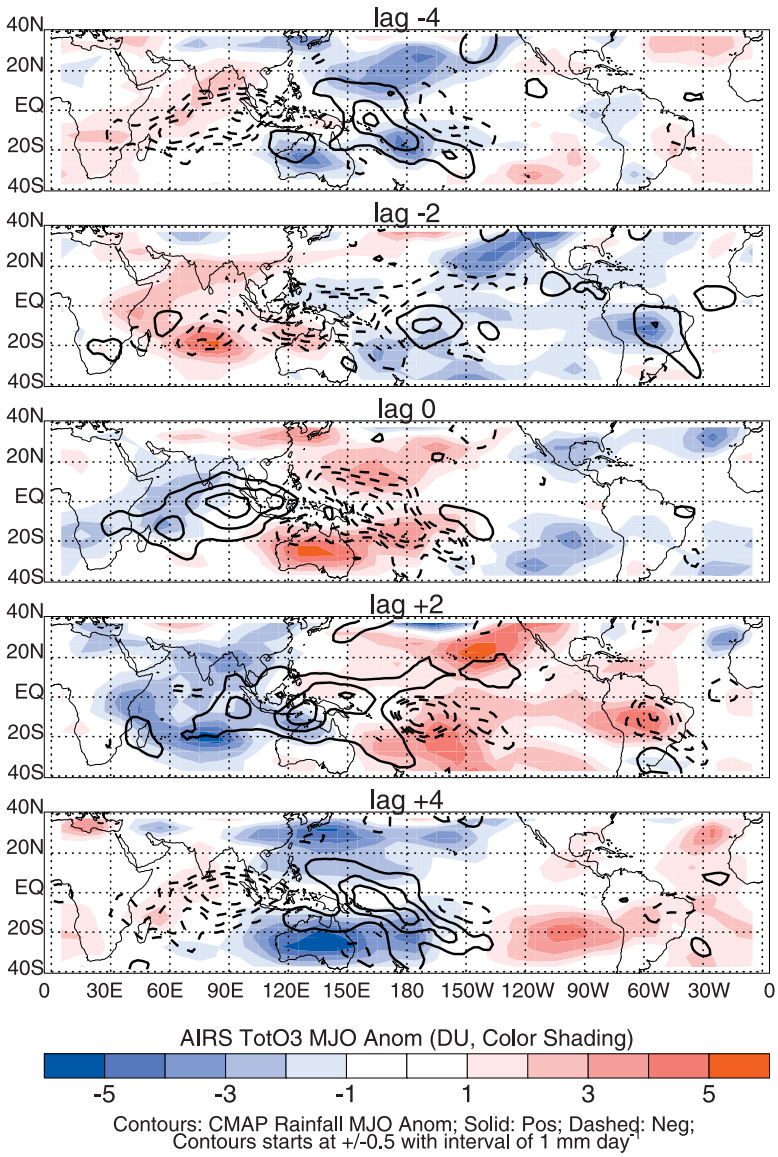

Figure 2. Same as for Figure 2 but for AIRS total O_3 MJO anomalies with different color scale.

structure of the MJO, an extended empirical orthogonal function (EEOF) was applied using time lags of ±5 pentads on boreal winter rainfall for the region 30°S–30°N and 30°E–150°W. Next, MJO events, 55 for MOD and 10 for AIRS (see Figure S1 of the auxiliary material for their dates),[1] were chosen based on the amplitude time series of the first EEOF mode of rainfall anomaly. For each selected MJO event, the corresponding 11-pentad rainfall, total O_3, geopotential height, and stream function anomalies were extracted for each data set (CMAP, MOD, AIRS, and NCEP). A composite MJO cycle (11 pentads) of anomalies was then obtained by averaging the selected MJO events.

3. Results and Discussion

3.1. Intraseasonal Variations of the Tropical Total O_3

[8] Figure 1 shows the horizontal maps of the MOD total O_3 anomalies for the composite MJO cycle with 95% confidence limits based on a Student's t-test. For simplicity, only lags ±4, ±2, and 0 pentads of the MJO cycle are shown. No spatial smoothing is used for the O_3 anomalies. Contour plots overlaid on the color shadings are the corresponding MJO-related CMAP rainfall anomalies. When calculating the statistical significance, we assume each MJO event to be independent and therefore counted as one degree of freedom. Note that the magnitude of the *composite* O_3 anomalies ranges up to about ±2.5 DU. However, inspection of individual events shows that they range up to about ±10 DU (~3% of the mean), but the compositing procedure reduces the signal amplitude. Thus, the intraseasonal variations of the tropical total O_3 are significant and comparable to those associated with other time scales, such as the annual cycle, QBO, ENSO, and solar cycle.

[9] Figure 1 indicates that large total O_3 variations (~±2.5 DU) are mainly found over the subtropical regions in the Pacific Ocean and the eastern hemisphere, most pronounced over the northern (winter) hemisphere. Over these regions, there exists a systematic relationship between

[1] Auxiliary materials are available in the HTML. doi:10.1029/2007GL029451.

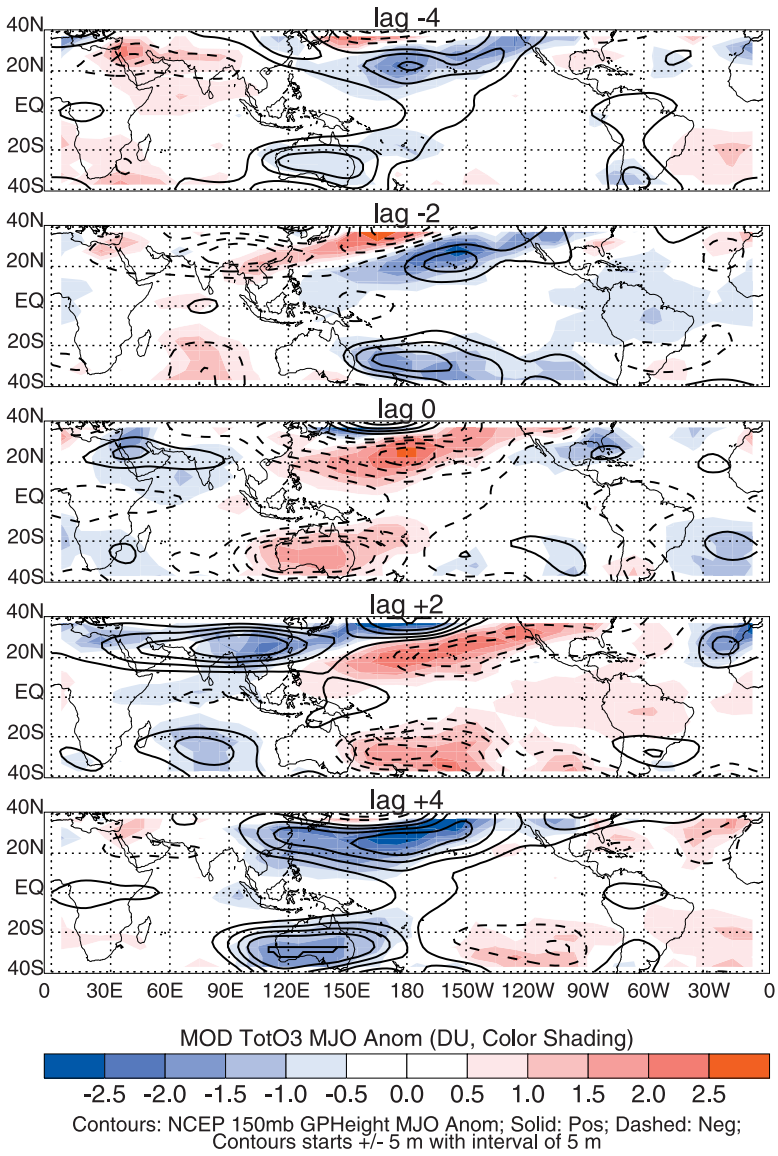

Figure 3. Composite MOD total O_3 (DU, color shading) and NCEP 150-hPa geopotential height (5 m, black contours) MJO anomalies.

the subtropical O_3 anomalies and the MJO convection anomaly over the equatorial Indian Ocean and western Pacific. The negative (positive) subtropical O_3 anomalies typically flank or lie to the west of enhanced (suppressed) equatorial MJO convection and propagate eastward at a phase speed of $\sim$5 m s^{-1} similar to the equatorial MJO convection anomaly. The subtropical O_3 anomalies maximize near 25° N and the dateline in the northwestern Pacific where MJO convection is located at the equatorial western Pacific. Over the equatorial regions (10°S–10°N), the O_3 variations are rather small (<1 DU) and considerably smaller than those at subtropical regions.

[10] Figure 2 presents the horizontal maps of the AIRS total O_3 MJO anomalies. Because of the small number of MJO events (10), we did not test the statistical significance of the AIRS O_3 anomalies. Comparison of Figures 1 and 2 indicates that AIRS and MOD O_3 anomalies have similar gross spatial and temporal patterns. For example, both MOD and AIRS indicate that O_3 anomalies are relatively large ($\sim\pm$5 DU) over the subtropics and relatively small over the equatorial regions. As with MOD, the AIRS subtropical O_3 anomalies also have a similar systematic relationship with the equatorial MJO convection discussed above. This indicates that the intraseasonal variations of the tropical total O_3, especially over the subtropics, and their relationship with the equatorial MJO convection are robust and not likely an artifact of the instruments or their samplings.

[11] However, the AIRS total O_3 anomalies are much larger ($\sim\pm$5 DU) than those in MOD and there also exist detailed differences in the spatial pattern. For example, at lags ±2, the MJO rainfall and O_3 anomalies extend further east over the northern Pacific in AIRS than MOD. Several factors may contribute to these differences. First, different MJO events are considered in MOD (55, from 1980 to 2006) and AIRS (10, from 2002 to 2006). More MJO events in MOD result in smaller O_3 anomalies in MOD because the compositing procedure reduces the signal amplitude.

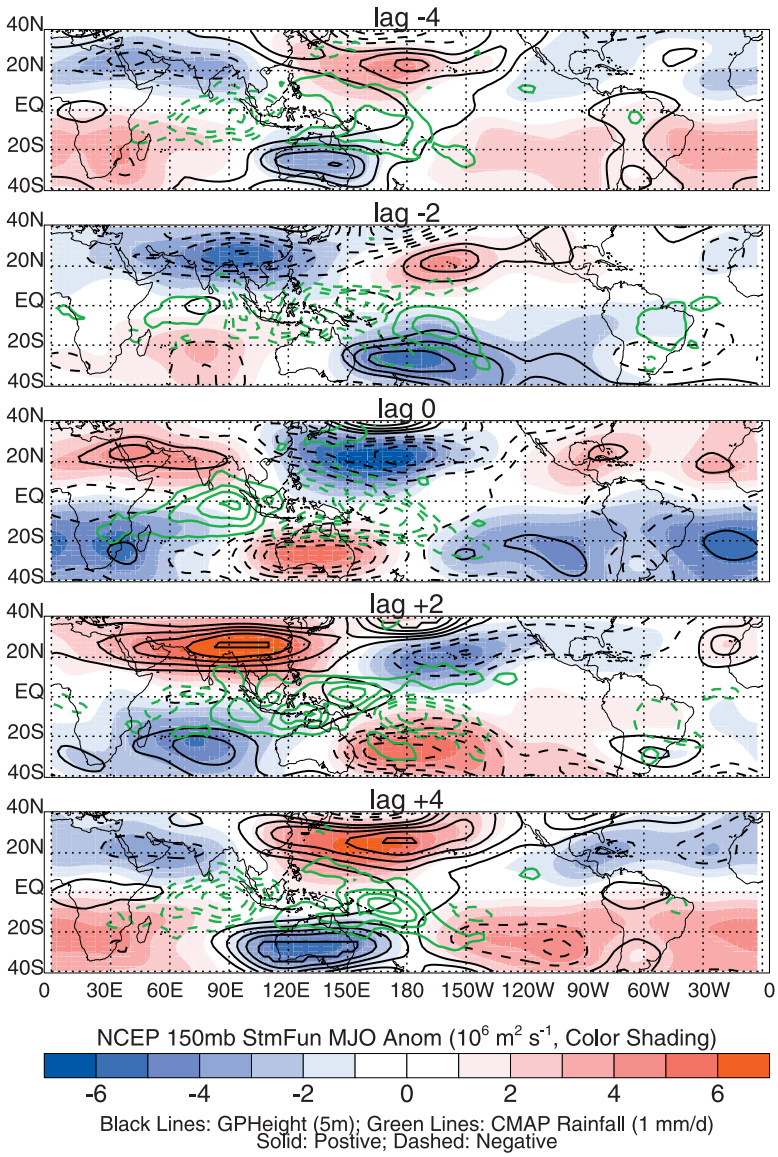

Figure 4. Composite NCEP 150-hPa stream function (10^6 m^2 s^{-1}, color shading), geopotential height (5 m, black contours), and CMAP rainfall (mm day^{-1}, green contours) MJO anomalies.

Different MJO events may also cause different spatial patterns of MJO convection and O_3 anomalies because MJO may vary in longer time scales. Direct comparison of the O_3 anomalies between MOD and AIRS using only data from the AIRS period (not shown) indicates a closer resemblance in both magnitude and spatial pattern and supports our reasoning. Second, MOD and AIRS use different retrieval techniques (UV backscatter for MOD and infrared emission for AIRS) and thus have different sampling characteristics (daytime for MOD and both day and night for AIRS). Third, both MOD and AIRS may have retrieval biases, especially over the equatorial regions where optically thick clouds are abundant associated with equatorial deep convection. For example, The TOMS is not sensitive to O_3 below optically thick clouds – and for cloud height they use climatology from the International Satellite Cloud Climatology Project [*Hsu et al.*, 1997]. This may cause large uncertainties in the total O_3 anomalies in MOD over the equatorial regions where optically thick clouds are high. However, the large MOD O_3 anomalies over the subtropics should not be affected by this bias because optically thick clouds are mostly absent there. The cloud clearing technique may also cause uncertainties in AIRS O_3 anomalies over the equatorial regions. But unlike TOMS which use a climatological cloud height, AIRS uses the in-situ cloud heights from the AIRS infrared measurements. Also, AIRS has some capabilities in retrieving O_3 below cloud tops in relatively cloudy conditions when effective cloud cover less than 70%. Thus, the AIRS O_3 may have more information than MOD over the equatorial regions. Fourth, AIRS seems to have more sensitivity than MOD as indicated by a still larger amplitude signal in AIRS in the two similarly sampled data sets.

3.2. Connection of the Total O_3 Anomalies to the MJO Dynamics

[12] It is well known that O_3 concentration is much higher in the stratosphere and much lower in the tropo-

sphere with a gradual transition at the tropical tropopause layer, bounded by the top of deep convective outflow near 150 hPa or 14 km and the cold-point tropopause near 80 hPa or 17 km [e.g., *Highwood and Hoskins*, 1998; *Folkins et al.*, 1999; *Sherwood and Dessler*, 2001]. Thus, any process that depresses the tropopause-layer height will tend to replace O_3-poor tropospheric air by O_3-rich stratospheric air, and the total O_3 will increase; and vice versa. This relationship has been shown at daily and synoptic time scales [e.g., *Reed*, 1950; *Schubert and Munteanu*, 1988; *Mote et al.*, 1991; *Salby and Callaghan*, 1993; *Steinbrecht et al.*, 1998]. To illustrate the role of the vertical movement of the tropopause layer in the intraseasonal total O_3 anomalies discussed above, we show the horizontal maps of the MOD O_3 (color shading, without confidence limit) and NCEP 150-hPa geopotential height (black contours) MJO anomalies in Figure 3. Figure 3 indicates that the subtropical total O_3 and 150-hPa geopotential height anomalies are highly anti-correlated (correlation coefficient of -0.88 for the latitude belt of $20-30°$N). Previous studies [e.g., *Kiladis et al.*, 2001] have shown that high/low geopotential heights near the tropopause are generally associated with a high/low tropopause-layer height on both intraseasonal and interannual time scales. This implies that the subtropical total O_3 anomalies at the intraseasonal time scale result mainly from the vertical movement of the tropopause, and thus are mainly associated with O_3 variability in the stratosphere rather the troposphere.

[13] To further elucidate the dynamical processes that cause the vertical movement of the tropopause layer that are responsible for the intraseasonal total O_3 anomalies over the subtropics, we present the horizontal maps of the NCEP 150-hPa stream function (color shading), geopotential height (black contours) and CMAP rainfall (green contours) MJO anomalies in Figure 4. Negative (positive) stream function values indicate a cyclone (an anticyclone) in the northern hemisphere but an anticyclone (a cyclone) in the southern hemisphere. In the eastern hemisphere and the Pacific Ocean, a subtropical anticyclonic (cyclonic) couplet near the tropopause flanks or lies to the west of enhanced (reduced) equatorial MJO convection and propagates eastward ($\sim$5 m s^{-1}) similar to the equatorial MJO convection anomaly (Figure 4). The subtropical anticyclones (cyclones) are most pronounced over the northern (winter) hemisphere. These UT large-scale MJO circulation features have been well documented and can be interpreted as an equatorial Rossby-Kelvin wave response to the equatorial MJO convection anomaly [e.g., *Rui and Wang*, 1990; *Hendon and Salby*, 1994; *Highwood and Hoskins*, 1998; *Kiladis et al.*, 2001]. Figure 4 indicates that negative (positive) subtropical geopotential height anomalies are typically collocated with the subtropical cyclones (anticyclones) near the tropopause. The correlation coefficient between geopotential height and stream function anomalies is $\sim$0.91 at the latitudes of $20-30°$S and $20-30°$N. This implies that the vertical movement of the subtropical tropopause layer that drives the subtropical total O_3 anomalies is a dynamical result of the subtropical cyclones or anticyclones near the tropopause, generated by the equatorial MJO convection anomaly.

[14] Over the equatorial regions, variations in geopotential height are dynamically constrained to be small (see Figures 3 and 4) [e.g., *Kiladis et al.*, 2001] and thus are not expected to play a dominant role in the equatorial total O_3 anomalies as in subtropics. The weak correlation coefficient (+0.28) between the equatorial MOD O_3 anomalies (<2.5 DU) and 150-hPa geopotential height anomalies (<10 m) further supports this point. Moreover, due to the direct influence of deep convection and the presence of water vapor and cloud anomalies, vertical mixing and chemical processes are likely to be important near the equator [*Jaegle et al.*, 2001]. Large uncertainties in MOD and AIRS O_3 retrievals over the equatorial regions due to the abundance of optically thick clouds further complicate this issue. Thus, the significance of the equatorial intraseasonal total O_3 anomalies, their origins (stratosphere or troposphere), and causes (dynamical or chemical) warrant further detailed satellite/in-situ data analyses and chemistry/transport modeling.

4. Conclusions

[15] In this paper, we document the spatial and temporal patterns of the tropical total O_3 intraseasonal variations and their connection to the large-scale MJO convection and circulation anomalies. Based on the MOD data, we found that the intraseasonal total O_3 anomalies are large ($\sim\pm$10 DU) and comparable to those associated with the annual cycle, QBO, ENSO, and solar cycle. The O_3 anomalies are mainly evident over the subtropics in the Pacific Ocean and the eastern hemisphere with a systematic relationship to MJO convection and dynamics. The subtropical positive (negative) O_3 anomalies flank or lie to the west of equatorial suppressed (enhanced) MJO convection and propagate slowly eastward ($\sim$5 m s^{-1}). The subtropical O_3 anomalies are typically collocated with the subtropical cyclones/anticyclones and are anti-correlated with geopotential height anomalies near the tropopause. This indicates that the subtropical total O_3 anomalies are dynamically driven by the vertical movement of the subtropical tropopause layer and mainly associated with the O_3 variability in the stratosphere rather the troposphere. Over the equatorial regions, the intraseasonal total O_3 anomalies are rather small (<1 DU) and may be a result of the coupled chemistry and dynamics of O_3. Similar intraseasonal variations of total O_3 in relation with the MJO are also found in AIRS with a relative short record. This indicates that the tropical total O_3 intraseasonal variations and their relationship with the equatorial MJO convection are robust. This study also demonstrates the potential for the AIRS O_3 to improve our understanding of O_3 chemistry and its effects on climate change. Finally, given that the potential predictability of the MJO extends to lead times of 2–4 weeks [*Waliser et al.*, 2003], the strong connection between the intraseasonal total O_3 variations and the MJO implies that the total O_3 variations may also be predictable with similar lead times over much of the tropics.

[16] **Acknowledgments.** This research was carried out at the JPL, Caltech, under a contract with NASA. It was jointly supported by the Research and Technology Development program, Human Resources Development fund, and the AIRS project at JPL. YLY and LK were supported by NASA grant NNG04GD76G to Caltech and TT acknowledged support by the Caltech SURF program in 2006. We thank S. Frith for sending us the daily TOMS/SBUV MOD data, R. Stolarski and X. Jiang for discussions and G. Kiladis for comments. The AIRS O_3, CMAP rainfall, and NCEP

reanalysis data are provided by NASA/GSFC/DAAC, NOAA/CPC, and NOAA/OAR/ESRL PSD from their web sites.

References

Bowman, K. P. (1989), Global patterns of the quasi-biennial oscillation in total ozone, *J. Atmos. Sci.*, *46*, 3328–3343.

Camp, C. D., M. S. Roulston, and Y. L. Yung (2003), Temporal and spatial patterns of the interannual variability of total ozone in the tropics, *J. Geophys. Res.*, *108*(D20), 4643, doi:10.1029/2001JD001504.

Chahine, M. T., et al. (2006), AIRS: Improving weather forecasting and providing new data on greenhouse gases, *Bull. Am. Meteorol. Soc.*, *87*, 911–926.

Folkins, I., M. Loewenstein, J. Podolske, S. J. Oltmans, and M. Proffitt (1999), A barrier to vertical mixing at 14 km in the tropics: Evidence from ozonesondes and aircraft measurements, *J. Geophys. Res.*, *104*, 22,095–22,102.

Fujiwara, M., K. Kita, and T. Ogawa (1998), Stratosphere-troposphere exchange of ozone associated with the equatorial Kelvin wave as observed with ozonesondes and rawinsondes, *J. Geophys. Res.*, *103*, 19,173–19,182.

Gao, X. H., and J. L. Stanford (1990), Low-frequency oscillations in total ozone measurements, *J. Geophys. Res.*, *95*, 13,797–13,806.

Gettelman, A., et al. (2004), Validation of Aqua satellite data in the upper troposphere and lower stratosphere with in situ aircraft instruments, *Geophys. Res. Lett.*, *31*, L22107, doi:10.1029/2004GL020730.

Hendon, H. H., and M. L. Salby (1994), The life cycle of the Madden-Julian Oscillation, *J. Atmos. Sci.*, *51*, 2225–2237.

Highwood, E. J., and B. J. Hoskins (1998), The tropical tropopause, *Q. J. R. Meteorol. Soc.*, *124*, 1579–1604.

Hood, L. L. (1997), The solar cycle variation of total ozone: Dynamical forcing in the lower stratosphere, *J. Geophys. Res.*, *102*, 1355–1370.

Hsu, N. C., R. D. McPeters, C. J. Seftor, and A. M. Thompson (1997), Effect of an improved cloud climatology on the total ozone mapping spectrometer total ozone retrieval, *J. Geophys. Res.*, *102*, 4247–4255.

Jaegle, L., D. J. Jacob, W. H. Brune, and P. O. Wennberg (2001), Chemistry of HOx radicals in the upper troposphere, *Atmos. Environ.*, *35*, 469–489.

Kiladis, G. N., K. H. Straub, G. C. Reid, and K. S. Gage (2001), Aspects of interannual and intraseasonal variability of the tropopause and lower stratosphere, *Q. J. R. Meteorol. Soc.*, *127*, 1961–1983.

Lau, K.-M., and D. E. Waliser (2005), *Intraseasonal Variability in the Atmosphere-Ocean Climate System*, 474 pp., Springer, New York.

Madden, R. A., and P. R. Julian (1972), Description of global scale circulation cells in the tropics with a 40–50 day period, *J. Atmos. Sci.*, *29*, 1109–1123.

Madden, R. A., and P. R. Julian (1994), Observations of the 40–50-day tropical oscillation: A review, *Mon. Weather Rev.*, *122*, 814–837.

Mote, P. W., J. R. Holton, and J. M. Wallace (1991), Variability in total ozone associated with baroclinic waves, *J. Atmos. Sci.*, *48*, 1900–1903.

Randel, W. J., and M. Park (2006), Deep convective influence on the Asian summer monsoon anticyclone and associated tracer variability observed with Atmospheric Infrared Sounder (AIRS), *J. Geophys. Res.*, *111*, D12314, doi:10.1029/2005JD006490.

Reed, R. J. (1950), The role of vertical motions in ozone-weather relationships, *J. Meteorol.*, *7*, 263–267.

Rui, H., and B. Wang (1990), Development characteristics and dynamical structure of tropical intraseasonal convection anomalies, *J. Atmos. Sci.*, *47*, 357–379.

Sabutis, J. L., J. L. Stanford, and K. P. Bowman (1987), Evidence for 35–50 day low frequency oscillations in total ozone mapping spectrometer data, *Geophys. Res. Lett.*, *14*, 945–947.

Salby, M. L., and P. F. Callaghan (1993), Fluctuations of total ozone and their relationship to stratospheric air motions, *J. Geophys. Res.*, *98*, 2715–2727.

Schubert, S. D., and M.-J. Munteanu (1988), An analysis of tropopause pressure and total ozone correlations, *Mon. Weather Rev.*, *116*, 569–582.

Sherwood, S. C., and A. E. Dessler (2001), A model for transport across the tropical tropopause, *J. Atmos. Sci.*, *58*, 765–779.

Shiotani, M. (1992), Annual, quasi-biennial, and El Niño-Southern Oscillation (ENSO) time-scale variations in equatorial total ozone, *J. Geophys. Res.*, *97*, 7625–7633.

Steinbrecht, W., H. Claude, U. Köhler, and K. P. Hoinka (1998), Correlations between tropopause height and total ozone: Implications for long-term changes, *J. Geophys. Res.*, *103*, 19,183–19,192.

Stolarski, R. S., and S. M. Frith (2006), Search for evidence of trend slowdown in the long-term TOMS/SBUV total ozone data record: The importance of instrument drift uncertainty, *Atmos. Chem. Phys.*, *6*, 4057–4065.

Stolarski, R. S., R. Bojkov, L. Bishop, C. Zerefos, J. Staehelin, and J. Zawodny (1992), Measured trends in stratospheric ozone, *Science*, *256*, 342–349.

Tian, B., D. E. Waliser, E. J. Fetzer, B. H. Lambrigtsen, Y. Yung, and B. Wang (2006), Vertical moist thermodynamic structure and spatial-temporal evolution of the MJO in AIRS observations, *J. Atmos. Sci.*, *63*, 2462–2485.

Waliser, D. E., K. M. Lau, W. Stern, and C. Jones (2003), Potential predictability of the Madden-Julian Oscillation, *Bull. Am. Meteorol. Soc.*, *84*, 33–50.

Ziemke, J. R., and S. Chandra (2003), A Madden-Julian Oscillation in tropospheric ozone, *Geophys. Res. Lett.*, *30*(23), 2182, doi:10.1029/2003GL018523.

E. J. Fetzer, F. W. Irion, B. Tian, and D. E. Waliser, Jet Propulsion Laboratory, California Institute of Technology, Mail Stop 183-501, 4800 Oak Grove Drive, Pasadena, CA 91109, USA. (baijun.tian@jpl.nasa.gov)

L. Kuai and Y. L. Yung, Division of Geological and Planetary Sciences, California Institute of Technology, Mail Stop 150-21, Pasadena, CA 91125, USA.

T. Tyranowski, Institute of Physics, Jagiellonian University, Reymonta 4, 30-059 Krakow, Poland.